Ultrasonics 82 (2018) 379–389

Contents lists available at ScienceDirect

Ultrasonics

journal homepage: www.elsevier.com/locate/ultras

Effect of microstructural elongation on backscattered field: Intensity measurement and multiple scattering estimation with a linear transducer array

Aurélien Baelde [a], Jérôme Laurent [a], Pierre Millien [a], Richard Coulette [b], Warida Ben Khalifa [b], Frédéric Jenson [c], Fan Sun [d], Mathias Fink [a], Claire Prada [a,*]

[a] ESPCI ParisTech, PSL Research University, CNRS, Institut Langevin, 1 rue Jussieu, F-75005 Paris, France
[b] Safran Aircraft Engines, Rond Point René Ravaud Réau, 77550 Moissy Cramayel, France
[c] Safran Tech, Rue des Jeunes Bois, 78772 Magny Les Hameaux, France
[d] PSL Research University, Chimie ParisTech - CNRS, Institut de Recherche de Chimie Paris, F-75005 Paris, France

ARTICLE INFO

Article history:
Received 17 May 2017
Received in revised form 30 August 2017
Accepted 4 September 2017
Available online 20 September 2017

ABSTRACT

The effect of microstructural elongation on ultrasonic backscattered fields was studied. Two methods for determining the elongation direction of macrozones in titanium alloys, using the anisotropic spatial coherence of the backscattered field, are presented. Both methods use a phased array attached on a rotative holder that records the array response matrix at several angles. Two titanium alloys were investigated: TA6V and Ti17. TA6V exhibited a strong macrozone elongation, whereas Ti17 macrozones were found equiaxial. The first method is based on the measurement of backscattered intensity in function of the probe angle relative to the macrozones elongation direction. An angular dependence of backscattered intensity is observed in presence of elongated scatterers, and their elongation direction is collinear with the probe direction corresponding to a minimal intensity. This variability is linked to both piezoelectric shape and the backscattered field spatial properties. The second method is based on the measurement of the relative proportion of single to multiple scattering in a diffusive media, using a simplified version of the single scattering filter developed in Aubry and Derode (2009). It allows the measurement of the level of multiple scattering: both titanium alloys exhibited strong multiple scattering. The elongation direction was determined as the direction of minimal multiple scattering. Furthermore, these results were confirmed by the measurement of the coherent backscattering cone on both samples.
© 2017 Elsevier B.V. All rights reserved.

1. Introduction

Titanium alloys are extensively used in the aerospace industry to create critical parts of jet engines or landing gears. They are light and very resistant to extreme conditions imposed to these parts. Titanium alloys are complex multiphasic polycrystals [1]. Their microstructures are extremely varied, leading to very different ultrasonic behaviours from one alloy to another. During ultrasonic evaluation, these alloys are known to present high levels of backscattered noise compared to other materials. This noise prevents the detection of low reflectivity and possibly harmful anomalies. Such anomalies are well known, for example, hard-α [2,3] or High Density Inclusion [4]. Ultrasonic evaluation can be carried out at two stages of the manufacturing process. The first stage is the billet stage: it is the raw titanium alloy forged in the shape of a long cylinder. The second stage is the forged part from the billet (disc, shaft). Due to safety high stakes in the jet engine industry, ultrasonic propagation has been extensively studied in polycrystals. The core of the structural noise generation is the scattering of wave on polycrystal's constitutive grains whose crystal orientation is different from one another. Early works [5–10] dealt with the measure and the theoretical computation of attenuation coefficients in polycrystals whose grains shape is equiaxial. All these studies were carried out using frequency domain hypothesis, relating wavelength with grain dimensions. Different expressions were derived for wave speed and attenuation in three frequency domains: Rayleigh for scatterers much smaller than wavelength, stochastic for scatterers whose size is comparable to wavelength and geometrical for scatterers bigger than wavelength. To overcome those frequency hypothesis, Stanke and Kino proposed a unified theory [11], still widely accepted and used, incorporating multiple scattering through the Keller approximation [12]. Another model was proposed by Hirsekorn [13,14], incorporating double

* Corresponding author.
E-mail address: claire.prada-julia@espci.fr (C. Prada).

https://doi.org/10.1016/j.ultras.2017.09.006
0041-624X/© 2017 Elsevier B.V. All rights reserved.

scattering. Nevertheless, this model exhibits non-physical "ripples" due to the choice of spheres as microstructure model. Multiple scattering was also taken into account by Weaver and Turner [15,16] by using the radiative transfer theory.

Thompson and his group carried out numerous experimental and computational studies on titanium alloys [17–24], and proposed models for the computation of scattering and attenuation coefficients. They introduced the key concept of figure-of-merit, also called backscattering coefficient, and proposed several methods for its measurement and computation. In the stochastic regime, they also demonstrated that polycrystals with elongated macrozones exhibit anisotropic behaviour of attenuation and backscattered noise intensity [23], but whose wave speed is still isotropic at their measurement precision. These apparently odd behaviours are dependent of both grain crystallographic orientation and shape. Alloys with elongated macrozones show high attenuation in the direction of grain elongation, along with weak backscattering. Inversely, they exhibit low attenuation and high backscattering while propagating perpendicular to the direction of grain elongation. Using the work of Thompson and Rose [25], Rokhlin confirmed theoretically the behaviour of backscattering [26,27] and attenuation [28,29] in elongated and equiaxial polycrystals in different crystal symmetries, taking into account both polycrystal texture and grain shape. Micro Textured Region (MTR) defined by Rohklin are similar to macrograins used in Thompson's work and to the concept macrozones used in European metallurgical vocabulary.

Recently, Dunne and Lowe used finite elements simulations to study the link between polycrystal texture and wave velocity [30]. Promising results were obtained by Van Pamel in using finite elements to predict attenuation and velocity in 3D polycristals, incorporating multiple scattering [31,32].

A straightforward macrostructure evaluation method have been introduced by Moreau [33,34] using a simple velocity measurement of millimetric slices of samples using a 10 MHz focused transducer. By spatially correlating velocity variations, he was able to measure effective velocity maps in the studied material. Macrozones were identified as area of similar velocities.

Although some studies demonstrated the existence of multiple scattering in titanium alloys [21,35] as deviation from an expected single scattering behaviour, most of the theoretical work relies on single scattering or low order multiple scattering hypothesis. When studying a novel material, it is important to determine if multiple scattering occurs in the desired frequency domain to properly design inspection using the appropriate theoretical propagation model.

Phased arrays are now widely used in medical ultrasound. Although less common in NDT, their potential is important. First, imaging techniques inspired from medical imaging can be directly transferred for the control of industrial materials. Moreover, Derode and Fink developed a method to determine fibers direction in composite material. This method relies on the difference of backscattered field spatial coherence at several fiber orientations [36]. However, the quick development of phased array has stimulated the creation of other methods, especially through matrix approaches of signal acquisition and processing [37]. Matrix approaches are based on the measurement of the array response matrix, also known as Full Matrix Capture. Imaging can still be performed in the matrix approach, generally referred to as "Total Focusing Method" [38]. Recently, Aubry and Derode proposed a matricial spatial coherence treatment to extract the single scattering contribution from the multiply scattered signals [39]. This method, strongly linked with the use of phased arrays, could be beneficial for the control of material presenting elongated microstructure. Moreover, phased arrays are composed of several piezoelectric elements, with specific shapes suitable to the phased array geometry. Piezoelectric element shape have an important impact on the measurement, and its influence on matrix method should be evaluated.

In this work, we demonstrate the use of transducer arrays for the determination of the direction of macrozones, taking into account single and multiple scattering properties of the backscattered field. Firstly, the microstructure of the titanium samples used in this study were characterized with optical and Electron Backscattering Diffraction (EBSD) measurements to highlight the macrozone shape. Then, the impact of the element shape on field integration and its use for elongation detection and characterization are presented. This method only uses the diagonal of the array response matrix. Secondly, we provide a method for multiple scattering estimation, using the whole measured array response matrix, and we analyze the influence of piezoelectric element shape on this method.

2. Samples characterization

First, the three samples types will be described. Then they will characterized using optical microscopy and EBSD. As ultrasonic waves are scattered by boundaries between macrozones, the aim of this part is to characterize the overall macrozone shape of our samples.

2.1. Samples

Three different media were studied Fig. 1. The first one, chosen as a prime example of anisotropic and diffusive medium is a collection of randomly placed, parallel steel rods [40]. Rod's diameter is 0.8 mm and the density of rods is 0.29 rods/mm^2. Steel rods are strong and elongated scatterers. This medium was studied by Tourin and Mamou [41–43] and used to demonstrate results on multiple scattering and coherent backscattering effect.

The two other samples are titanium alloy half billets. A billet is a cylinder used as raw material by engines manufacturers. Two titanium alloys were studied: TA6V and Ti17. Each billet was cut in half along the plane containing its revolution axis, leading to four half cylinders, two of TA6V and two of Ti17 (radius: 130 mm, length: 269 mm). These two alloys are known to present different microstructures that will be studied further.

Studies showed that effective ultrasonic longitudinal wave velocity in titanium alloys are comprised between 6.0 mm/μs and 6.35 mm/μs [44]. Typical wavelength will range from 1.5 mm to 6 mm in the selected frequency domain. As ultrasonic wave interact with scatterers of size within three orders of magnitude compared to its wavelength. Material characterizations should be done in the micro-millimetric domain, which is the relevant scale for ultrasonic scattering at our experiment frequency domain. This is also a scale generally used in other studies [17].

2.2. Characterization of titanium alloys

Titanium samples were characterized using classic Optical Microscopy and EBSD. Samples were cubes of 13 mm side extracted from the TA6V and Ti17 billets. Samples were first polished until reaching a mirror-like surface. For optical microscopy, surfaces were then exposed to a mixture of fluoridric acid and nitric acid during 10 s (1%HF, 3%HNO3).

First, optical microscopy was performed with a Keyence VHX-500 microscope. Optical contrast is sensitive to both crystallographic phase and crystallographic orientation. In a second step, samples were polished again to a mirror like surface and observed with a Zeiss Leo 1530 electronic microscope using an EBSD head. The accelerating voltage was 20 kV, the working distance

Fig. 1. Samples used for the experiments: (a) collection of randomly placed parallel rods called Random Rod Forest, (b) two half billets of TA6V and Ti17 titanium alloys.

14.8 mm and tilt angle 70.0°. The EBSD contrast is also sensitive to crystallographic phase and orientation, but phase identification is possible as Kikuchi diffraction pattern are related to crystallographic arrangement [45].

Elongated macrozones are observed in TA6V samples Fig. 2(a) as bright areas on the image. A macrozone is a group of several α grains having approximately the same crystallographic orientation. The shape of macrozone is elongated polygons measuring $10 \times 1\ \mathrm{mm}^2$ on average. The elongation direction is parallel to the billet axis. This elongation is attributed to the forging process: titanium alloys forged in the $\alpha + \beta$ domain undergo few recrystallization in the last forging step. Therefore, macrozone's shape conform to the plastic deformation applied in the final step of the forging process. The Ti17 presents equiaxial macrozones Fig. 2(b): they are not elongated, and their average size is 0.7 mm. Ti17 billets are forged in the β domain: recrystallization occurs after the last deformation is applied. This lead to the most thermodynamically stable macrostructure: equiaxial macrozones.

To confirm optical microscopy results on α phase orientation, an EBSD experiment was carried out on the same samples on a surface of $1 \times 1\ \mathrm{mm}^2$. EBSD image colored pixels indicate the α-phase orientation while non-indexed β-phase is represented by black pixels.

EBSD measurements presented in Fig. 2(c) and (d) show large areas of similar crystallographic orientation for TA6V alloy. These areas are composed of smaller equiaxial α grains, all with similar crystallographic orientation. As expected, macrozones are composed of several α grains all with a common crystallographic orientation. These α grains are recrystallized from previous α platelets

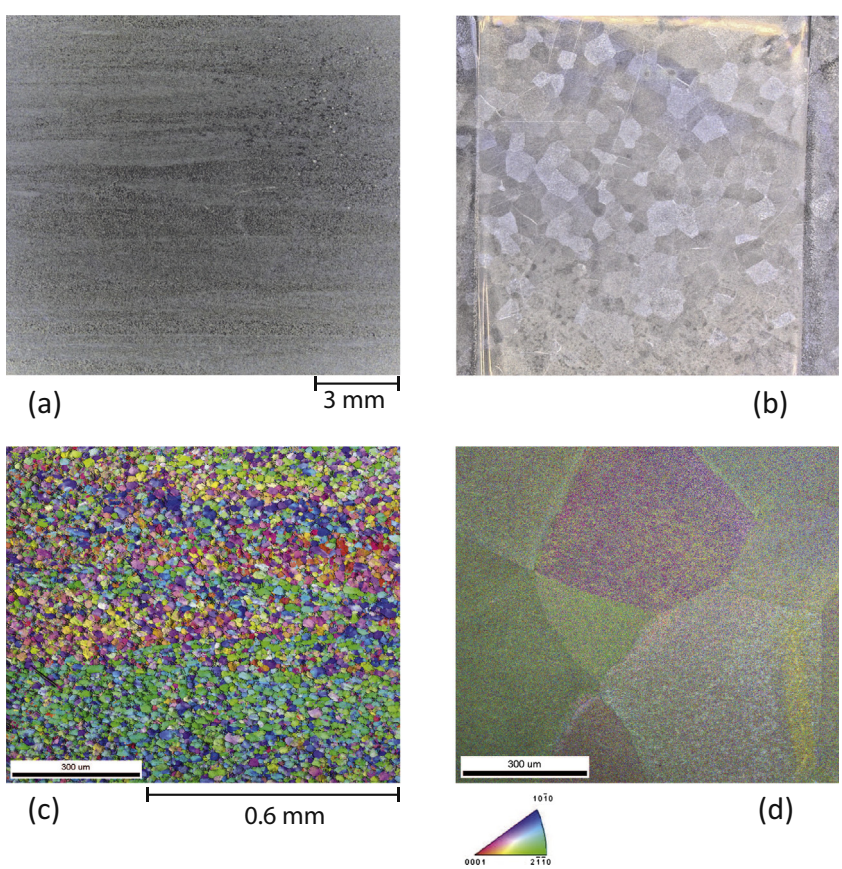

Fig. 2. Billet characterization using optical microscopy and EBSD. Optical microscopy is used on (a) TA6V and (b) Ti17. The length scale is the same for both images. EBSD is applied on (c) TA6V and (d) Ti17. The length scale is the same for both images but different from optical microscopy. The elongation direction of TA6V macrozones is parallel to the billet revolution axis.

destroyed by the forging and merged into equiaxial α grains. On the other hand, Ti17 alloy exhibits large equiaxial area of common crystallographic orientations, consistent with optical microscopy observations Fig. 2(d). No substructure is visible at this magnification. A noise is visible inside macrozones, probably linked to micrometric α platelets with variants in orientation.

In summary, alloys used in this study differs by the shape of their microstructure: TA6V is formed of elongated macrozones along the billet axis and Ti17 is composed of equiaxial macrozones.

3. Experimental setup

A linear 128 elements phased array has been used to illuminate the samples. Nominal frequency of piezoelectric elements is 3.5 MHz. They are separated by a pitch of 0.417 mm without focalization lens. Piezoelectric elements have a rectangular shape of 10 mm height and 0.4 mm width. The phased array probe is controlled by a LeCoeur (OPEN System) 128 independent channels pre-amplifier using arbitrary signal generator and a gain of 80 dB. Each element of the phased array can be independently excited by arbitrary signals. Signals were sampled at 80 MHz. The probe was mounted on a rotating stage, allowing it to turn around its axis as defined in Fig. 3. Sample are placed in front of the array. The probe sample distance is 65 mm. The half cylinders radius is 130 mm and their length is 269 mm. According to the array design, ultrasonic characterization will be carried out in the frequency bandwidth [1–4] MHz.

The array response matrix was measured. Let's denote $k_{ij}(t)$ the temporal signal recorded on channel i, after emission by channel j. The array response matrix is a $N \times N$ matrix of element $k_{ij}(t)$, where N the number of transducers in the array. In this study, a temporal slice of the matrix is denoted $K_{ij}^{T}(t)$ and defined by the portion of matrix included in the duration $[T - \Delta t/2,\ T + \Delta t/2]$. The duration Δt is implicit in the notation T that will be referred to as the "time window".

Signals can be transformed in the Fourier space using Fast Fourier Transform. The sliced array response matrix can be expressed in the frequency space as

$$K_{ij}^{T}(\omega) = \frac{1}{\sqrt{2\pi}} \int_{-\infty}^{\infty} k_{ij}^{T}(t) e^{\mathbf{i}\omega t} \mathrm{d}t. \tag{1}$$

Due to the reciprocity theorem, the array response matrix is symmetric: $K_{ij} = K_{ji}$.

4. Backscattered intensity measured by a single element

First, a single element approach was used. This section provide a method for determining macrozone elongation direction using the measurement of backscattered intensity with a rectangular shaped transducer. Backscattered intensity from polycrystals has been measured and modelled by several authors. Their work generally dealt with the computation of the backscattering coefficient, which is the backward differential cross section of the medium, as a function of the wave vector and the material spatial correlation function. These approaches took into account the transducer shape [46–48] but not the ultrasonic field spatial coherence.

The 'single element' terminology refers to the fact that only one element of the transducer is used to emit and record the ultrasonic amplitude. This experiment could be carried out using a single standalone transducer and it do not use the spatial sampling capabilities of a phased array probe. The medium position is set and only the transducer is rotated along its axis defined in Fig. 3. At different angles, the wave field will interact of different manners with the medium, especially in terms of spatial coherence and field integration on the transducer. Each element produced a pulse signal centered at 3.5 MHz of duration 0.73 µs multiplied by a temporal Hanning window. The gain amplification of the LeCoeur device was set near 75 dB, in order to measure the structural noise. As a consequence, the water/titanium interface echo was saturated. The usable signal were only available after 20 µs of propagation in the titanium samples.

The samples were insonified through their plane interface. For each array angle θ, the array response matrix was recorded. The sliced array response matrix is denoted $K_{ij}^{T,\theta}(\omega)$.

The backscattered intensity recorded at angle θ, at frequency ω, on element i is

$$I_i^{T,\theta}(\omega) = \left| K_{ii}^{T,\theta}(\omega) \right|^2. \tag{2}$$

The averaged backscattered intensity at angle θ was computed over all array elements as

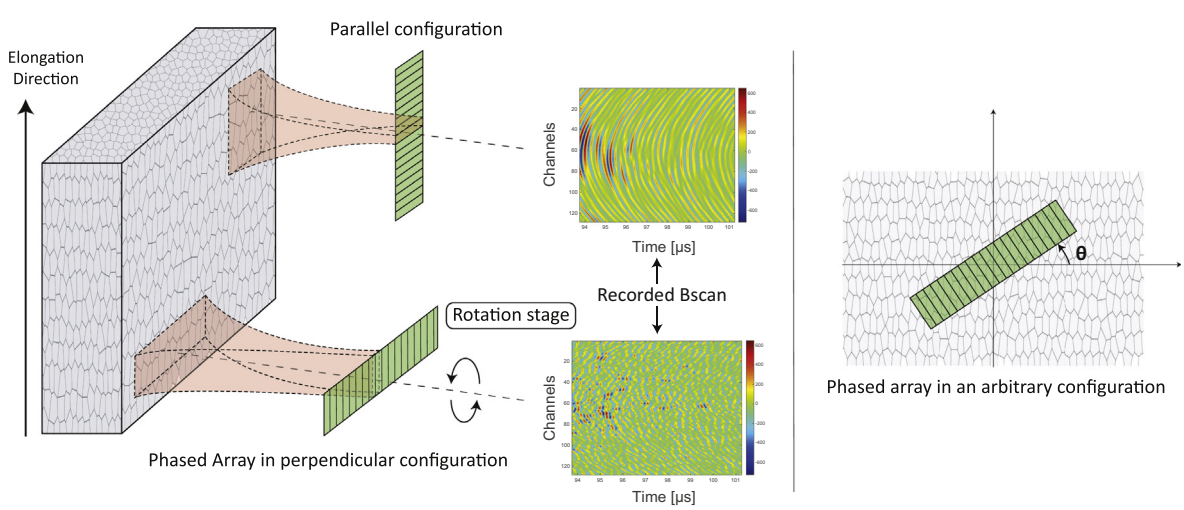

Fig. 3. All samples are placed with vertical elongation direction. Likewise, billets revolution axis is oriented vertically. The probe is mounted on a rotation stage in front of the sample. It can rotate around its central element. The bottom configuration is called perpendicular, as the elements aligning direction is perpendicular to the sample microstructure elongation. In the upper configuration called parallel, the probe is rotated of 90°. In both configurations, a Bscan recorded in a random rod forest is provided to show the difference in field spatial coherence between configurations. In practice, the phased array probe can rotate of an arbitrary angle denoted θ.

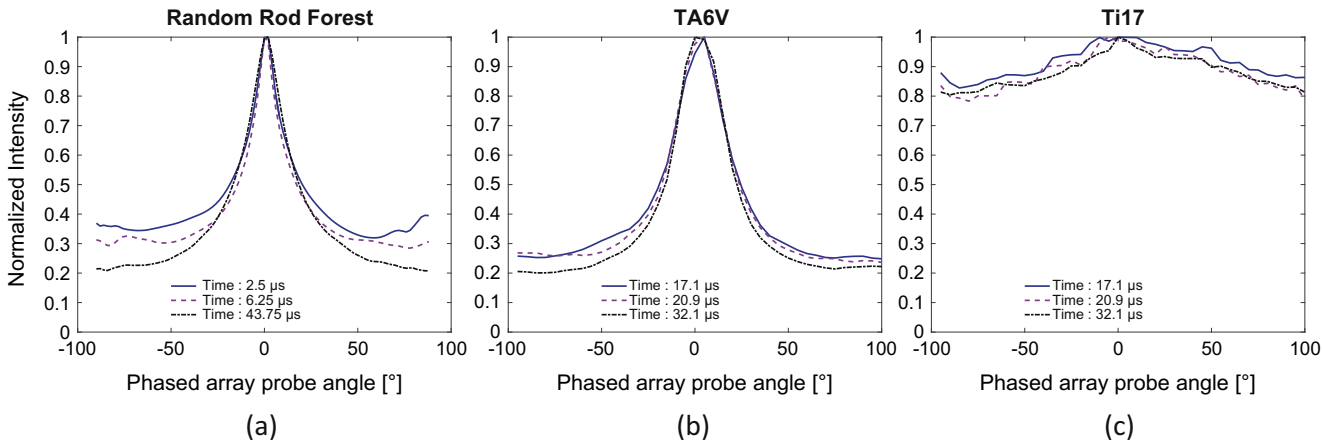

Fig. 4. Normalized average intensity as a function of probe angle for (a) the random collection of parallel rods, (b) the TA6V and (c) the Ti17. The time window length is 2.5 µs and signals are filtered to keep the [3–4] MHz frequency bandwidth. $\theta = 0^\circ$ corresponds to the perpendicular configuration of the probe, $\theta = 90^\circ$ corresponds to the parallel configuration of the probe.

$$I^{T,\theta}(\omega) = \frac{1}{N}\sum_{i=1}^{N} I_i^{T,\theta}, \tag{3}$$

were N is the number of array elements. In the experiment, the duration of a temporal window is 2.5 µs.

In Fig. 4, $\theta = 0^\circ$ corresponds to the perpendicular configuration of the probe, $\theta = 90^\circ$ corresponds to the parallel configuration of the probe.

Backscattered intensity from the rod forest is maximum in the perpendicular configuration and minimum in the parallel one. The elongation of rods is visible through the difference of intensity between the perpendicular and parallel configurations. A similar result is observed on the TA6V billet. Scatterers embedded in the TA6V microstructure are elongated along the billet revolution axis. This is in accordance with characterizations made before: TA6V macrozones are elongated along the billet axis.

In Ti17, the backscattered intensity weakly depends on the probe angle. This is consistent with the Ti17 characterization: its macrozones are almost equiaxial.

The measurement of the averaged backscattered intensity is a practical way to detect and determine the elongation direction of scatterers. In these examples, the maximum backscattered intensity is reached when the individual elements elongation is parallel to microstructure elongation.

How can we explain this result? — First, the elongation of scatterers plays a central role. More precisely, the backscattered field from the elongated scatterers presents an anisotropic spatial coherence. In the case of rods, the field is strongly incoherent in the plan perpendicular to their elongation direction (transverse plane): the field is the superposition of numerous wavelets scattered by randomly placed scatterers. As the scatterers are randomly placed, the superposition of wavelets amplitude is also random and leads to the random pattern. On the elongation dimension, rods backscatter a very coherent field: they behave like a mirror in this dimension. In this dimension, incident wave vectors are backpropagated without interference, which lead to a very coherent wave front. Fig. 5 gives a graphical explanation of this phenomenon. In the case of spherical scatterers, whatever the transducer shape, the experiment is invariant by rotation of the probe. This is what is observed in Ti17: macrozones are roughly equiaxial. The experiment is invariant by rotation of the probe, even if the transducer is rectangular. In reality, macrozones are not perfectly circular and can be slightly elongated. This is observed in the small variability of the Ti17 intensity curve.

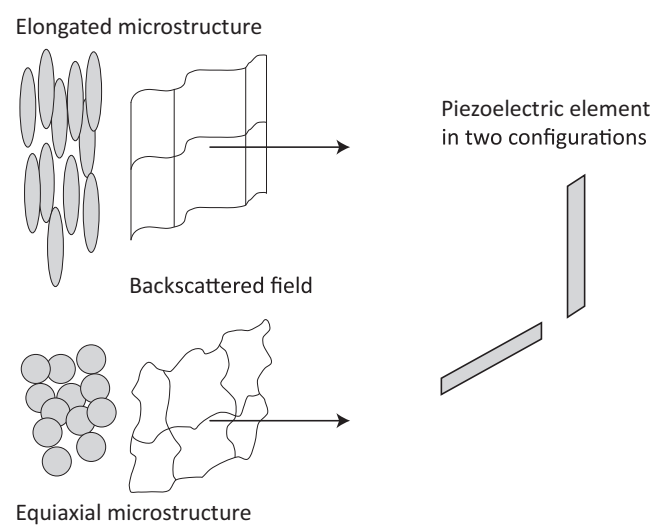

Fig. 5. An idealized surface of equal phase of the backscattered field is drawn for two types of microstructure elongated (top) equiaxial (bottom). In elongated microstructure, the field is more coherent in the elongation plane than in the transverse plane. In the equiaxial microstructure, the field spatial coherence is isotropic. (right) Two orientations of a single piezoelectric element of the phased array are drawn. The field integrated on the element surface depends on the element shape and the elongation direction relative to the element.

Second, a non-circular shape of the piezoelectric elements is necessary. If the elements were circular, the experiment would not depend on the probe rotation, while for a non-circular element and elongated scatterers, the dependence can be observed. The intensity measured on the element is the square of the signal recorded on the piezoelectric element. This measured signal is proportional to the average pressure on the element. As stated before, if scatterers are elongated, the field presents an anisotropic spatial coherence. Using a non-circular transducer, the pressure will not be integrated in the same way depending on the relative orientation of field spatial coherence anisotropy and the transducer symmetry axis. The rectangular transducer is symmetric by rotation of 180°, meaning that field integration on the transducer has a periodicity of 180°. A square transducer will lead to a 90° periodicity.

Furthermore, the relative size of macrozones and grains compared to the wave length is important. In facts, α-grains size is approximately 20 µm and macrozones size is from 100 µm to 1000 µm since wavelength is 1700 µm at 3.5 MHz. The interaction

of ultrasound with macrozones is far greater than its interaction with grains. As the elongation is linked to the fact that several grains share the same crystallographic orientation within a single macrozones, the ultrasonic behaviour is more influenced by the macrozones, which have a size similar to wavelength, than the individual grains which are much smaller. This relative influence of grains and macrozones on ultrasonic propagation was studied by Ahmed and Anderson [49] and Rokhlin [50].

One advantage of this method is that only one face of the sample needs to be accessible, contrary to methods involving attenuation or backscattering coefficient with circular transducers that need at least two inspections directions.

5. Anisotropy detection using multiple scattering measurement

In the previous section, only diagonal elements of the array response matrix have been used. This is equivalent to use a single transducer and average results on several medium random configuration. But, the whole matrix contains more information than the average of single transducer measurements. Specifically, it allows the simultaneous spatial sampling of the wave field, leading to the possibility to evaluate the wave field coherence. This is the idea of the Multiple Scattering Filter (MSF) developed by Aubry and Derode [39]. They demonstrated that the array response matrix shape depends on the scattering regime occurring in the medium. In the following section, we modified this filter to quantify the relative importance of each scattering regime at any time. Then, we used this tool as a way to probe scatterers elongation, relying on the difference of multiple scattering development speed in the sample. This can be understood in the rod forest: multiple scattering rapidly occurs in the transverse plane but develops very slowly in the vertical plane.

5.1. New expression of single scattering estimator and quality estimation

Aubry and Derode used the array response matrix singular value probability distribution as an indicator of the scattering regime in the sample. This indicator is reliable but suffers from the high number of averages (frequency, time, sample realization) needed to compute a reliable estimator of the singular value distribution. Moreover, at a given frequency, the array response matrix exhibits different forms in single or multiple scattering as highlighted in Fig. 6. This matrix form is described by the expression derived by Aubry [39] For single scattering with the paraxial approximation, the matrix's anti-diagonals obeys a specific phase law, whereas diagonals are multiplied by a random value

$$k_{ij}(T,f) \sim \underbrace{\frac{\exp(\mathbf{j}2kR)}{R}\exp\left(\mathbf{j}k\frac{[(x_i-x_j)p]^2}{4R}\right)}_{\text{phase law}}\underbrace{\sum_{d=1}^{N_d} A_d \exp\left(\mathbf{j}k\frac{(x_i+x_j-2X_d)^2}{4R}\right)}_{\text{random term}}, \tag{4}$$

where first term is the phase law and the second term is the random multiplier. R is the probe-sample distance, k the wave vector, p the array pitch, x_i and x_j the i and j elements position, A_d the dth scatterer's scattering amplitude and X_d the dth scatterer position.

If multiple scattering dominates, the array response matrix is random and its coefficients follow a Gaussian distribution.

To simplify the multiple scattering estimator proposed by Aubry and Derode, we consider a matrix subspace containing the single scattering matrix described in Eq. (4). Then the experimental matrix is projected on this *a priori* known subspace to measure its difference with the theoretical single scattering matrix.

The first step is to model the single scattering space. This space is spanned by the matrix E_k defined as

$$E_k(i,j) = \begin{cases} 0 & \text{if} \quad i+j \neq k+1 \\ g(i-j)/\sqrt{P(k)} & \text{if} \quad i+j = k+1 \end{cases}, \tag{5}$$

with $g(i-j) = \exp\left(\mathbf{j}k((i-j)p)^2/(4R)\right)$ and

$$P(k) = \begin{cases} k & \text{for} \quad k \leq N \\ 2N-k & \text{for} \quad N < k < 2N \end{cases}. \tag{6}$$

A single scattering matrix is a vector of this subspace, as it can be written as a linear combination

$$K^S = \sum_{k=1}^{2N-1} a_k E_k, \tag{7}$$

where a_k is a complex random vector.

The matrix E_k represents the kth anti-diagonal of the single scattering matrix.

Experimental matrices are symmetric, due to the reciprocity theorem. The symmetric matrices space is of dimension $N(N+1)/2$ whereas the single scattering space dimension is $2N-1$. The higher N, the smaller is the single scattering space compared to the whole space.

The Frobenius norm and its scalar product are associated to the subspace. Using this definition, the matrix base is orthonormal

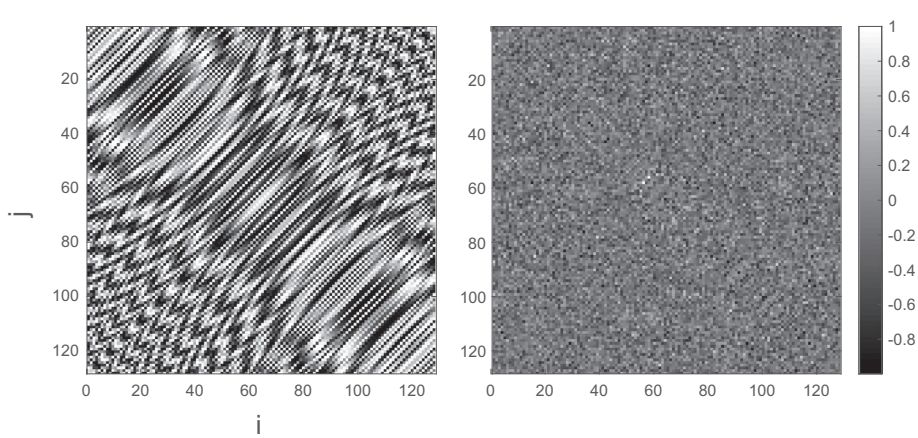

Fig. 6. (a) Real part of a simulated array response matrix in the single scattering regime in water, at frequency 3 MHz and at a distance of point scatterers of 200 mm, for a 128 elements phased array whose element pitch is 0.417 mm, (b) Simulated array response matrix in the multiple scattering regime.

$$\langle E_k, E_j \rangle = \begin{cases} 0 & \text{if } k \neq j \\ 1 & \text{if } k = j \end{cases}, \tag{8}$$

The experimental matrix, denoted K_{exp} is normalized using the scalar product defined before

$$\widetilde{K}_{exp} = \frac{K_{exp}}{\|K_{exp}\|}. \tag{9}$$

The experimental matrix can be projected on the E_k basis as

$$pK = \sum_{k=1}^{2N-1} \langle \widetilde{K}_{exp}, E_k \rangle E_k. \tag{10}$$

The projection norm is written as

$$p^E = \sqrt{\sum\nolimits_{k=1}^{M} |\langle \widetilde{K}_{exp}, E_k \rangle|^2}. \tag{11}$$

The quantity p^E is the norm of the projection of the experimental matrix on the single scattering space. It is expected to be an estimator of the single scattering proportion. The next section is devoted to the study of the quality of this estimator.

5.1.1. Estimator quality

In order to evaluate the validity of this single scattering proportion estimator, it is tested on synthetic array response matrices defined as

$$K_{exp} = SK^S + MX. \tag{12}$$

where S and M are the single and multiple scattering relative amplitudes, respecting the condition $S + M = 1$. K^S is the normalized single scattering matrix and X is a normalized random Gaussian matrix, symmetric to mimic the reciprocity theorem.

The single scattering proportion estimator is written as

$$p^E = \frac{1}{\|SK^S + MX\|} \sqrt{\sum\nolimits_k \left| S\langle K^S, E_k \rangle + M\langle X, E_k \rangle \right|^2}. \tag{13}$$

As the multiple scattering matrix is not orthogonal to the single scattering sub-space, p^E is not strictly equal to the single scattering proportion defined as

$$p^S = \frac{\|SK^S\|}{\|SK^S + MX\|} = \frac{S}{\|SK^S + MX\|}. \tag{14}$$

In order to evaluate this estimator, we calculate the discrepancy between the single scattering proportion p^S and its estimation p^E.

Eq. (13) has been evaluated for p^S ranging from 0 to 1, for several realizations of K^S and X. Fig. 7 displays the discrepancy between the desired quantity (p^S) and the one that is actually measured (p^E).

Fig. 7 demonstrates that p^E is a very good estimator if single scattering proportion is high. The estimator deviates significantly at low values of single scattering proportion: this is the residual of the projection of multiple scattering on the single scattering subspace. This residual decreases as probes' number of elements increases. According to Eq. (13), the estimated single scattering proportion is 1 when the true proportion is 1. When the single scattering proportion is 0, the residual is

$$p^S(p^E = 0) = E\left[\sqrt{\sum\nolimits_k |\langle X, E_k \rangle|^2}\right]. \tag{15}$$

5.1.2. Single scattering proportion on a random rod forest and titanium alloys

The method was first tested in a random rod forest and then was applied to the titanium alloys studied earlier, to quantify the time and angular dependence of single scattering. For each probe angle, an array response matrix was measured using the same parameter than in the previous section and post-processed using the single scattering proportion estimation method explained earlier. The array response matrix was sliced in 5 µs time windows whose center are separated by 1.25 µs. The probe sample distance is 65 mm. After post-processing, single scattering proportion curves were frequency averaged in the 3–4 MHz bandwidth.

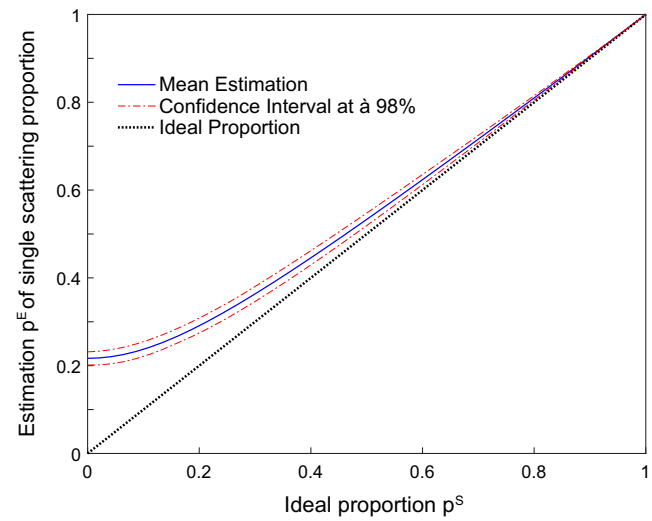

Fig. 7. Estimation of single scattering proportion p^E on simulated matrices of controlled single scattering proportion p^S. The estimator (solid) is linear at high single scattering proportion, exhibit weak variability (dashed-dotted) and diverge from the ideal estimator (dotted) at low single scattering proportion.

Fig. 8 represents the time and angle dependence of single scattering proportion in three samples: random rod forest, TA6V and Ti17. In the random rod forest, the single scattering proportion is decreasing faster if the probe is perpendicular to the rods than if the probe is parallel. Multiple scattering develops quicker in the perpendicular configuration. This result is confirmed by the angular dependence. At early time, single scattering dominates whatever the angle. At later time, multiple scattering appeared more rapidly in the perpendicular configuration than the parallel. This results is twofold: multiple scattering is observed and measured, and multiple scattering does not develop at the same speed depending on the relative angle between the probe and the rod elongation direction.

A similar behaviour is observed in TA6V. Early times are not available due to the high amplitude of interface echo, multiple scattering is the highest in the perpendicular configuration, and at a given time, decreases as the probe rotates from this maximum multiple scattering configuration. Scatterers elongation is observed through the variability of single scattering proportion measurement. It should be noted that the maximum multiple scattering configuration correspond to angle of maximum intensity in the previous experiment. The common origin of these two phenomenon is the elongated shape of scatterers.

Ti17 exhibit strong multiple scattering and no dependence with probe angle. This is consistent with its equiaxial macrozones: the medium is statistically invariant for probe rotation. This doesn't mean that multiple scattering propagation is isotropic, but it means that whatever the probe angle, multiple scattering will develop in the same way.

Multiple scattering does not depend on the transducer, it depend on the medium properties. In a rod forest, multiple scattering develops quicker in the transverse plane than in the vertical plan. The field radiated by a rectangular element is not isotropic: the medium is not excited the same way depending on the probe angle and the recorded field also depends on the probe angle. This

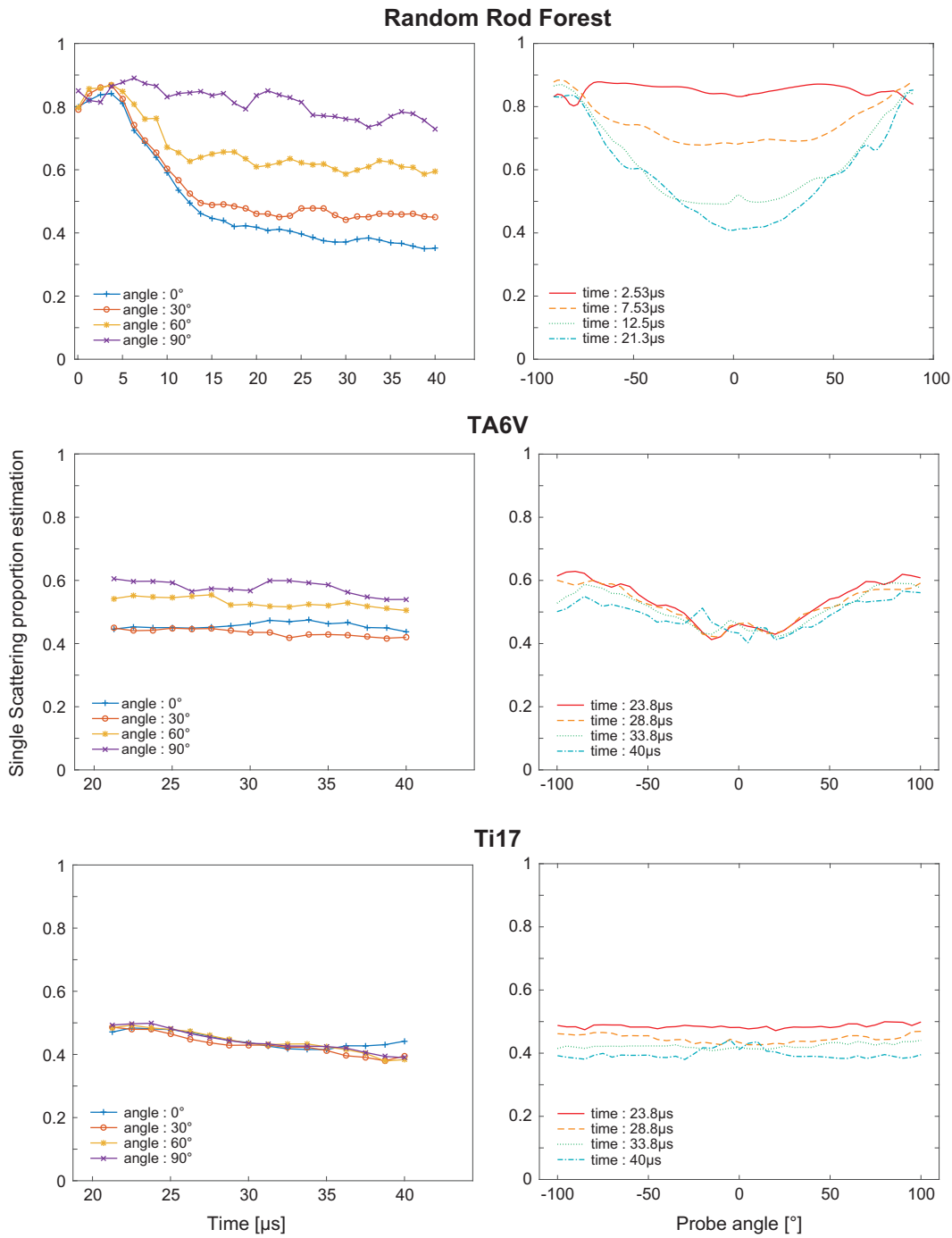

Fig. 8. Single scattering proportion as a function of time (left column) and as a function of probe angle (right column) for the random rod forest (top line), TA6V (middle) and Ti17 (bottom). In the random rod forest, single scattering proportion decreases over time and decreases more quickly in the perpendicular configuration. In the TA6V, the single scattering proportion is constant at later times (>20 μs) but weaker in the perpendicular direction. In Ti17, single scattering proportion is decreases slightly over time but does not depend on probe angle.

is illustrated by Fig. 9. In the perpendicular direction, elements sample multiple scattering very well on their thin dimension and integrate a rather coherent field on their long dimension. In the parallel configuration, multiple scattering is integrated on the long dimension and the coherent part of the field is sampled.

Moreover, backscattered intensity measurements was performed with only one transducer element and strongly depends on its shape. But the multiple scattering estimator relies on the field coherence spatially sampled by a plurality of transducers, which is the major difference between both methods. Stated differently, backscattered intensity uses only the array response matrix diagonals, and single scattering estimator uses the whole matrix, therefore exploiting more information. Backscattered intensity is driven by element shape, and the multiple scattering estimation is driven by the phase relation between several elements.

Contrary to backscattering intensity measurements, the single scattering estimator seems less robust to detect the elongation direction. The single scattering estimation is very sensitive to measurement artefact, as it uses the matrix shape to compute single scattering proportion. All phased array elements are used to record the array response matrix and compute the single scattering proportion: the area inspected is defined by the beam width of all elements.

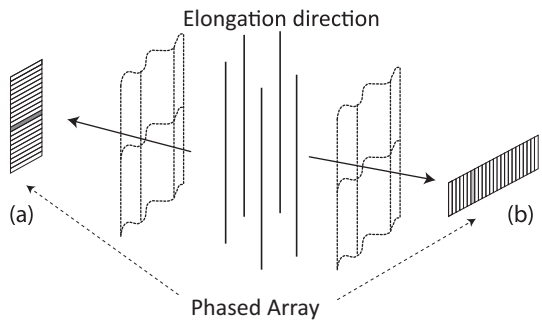

Fig. 9. Field integration on the phased array probe in two different configurations. (a) Elements integrate the incoherent field on their long dimension and the phased array samples the field along the coherent dimension: the effective field measured exhibit a large portion of single scattering. (b) Elements integrate the coherent field along their long dimension and the phased array sample the field on the incoherent dimension: if the medium is strongly scattering, the effective field measured exhibits a small proportion of single scattering.

As the field radiated by rectangular elements can be wide, the usable surface (no edges or scattering geometrical shape) of the sample must large. This prevents the method in its present form to be used on samples smaller than the phased array total active surface.

5.2. Coherent backscattering cone

The coherent backscattering effect is a signature of multiple scattering. This effect is the consequence of the constructive interference of waves following reciprocal paths. The core concepts of coherent backscattering are recalled here. Additional details can be found in [51–54,43].

When a wave propagates in a scattering media from a point source S to a receiver R, the field recorded on R at a given time t is the superposition of numerous scattering paths followed by the wave to propagate from S to R. Denoting a particular path p, the intensity recorded on R can be written as

$$I(R,S,t) = \sum_p |A_p|^2 + \sum_p \sum_{q \neq p} A_p A_q^* = I_{inc}(R,S,t) + I_{coh}(R,S,t). \quad (16)$$

The first term is called "incoherent" intensity. It is the addition of the intensities associated with all possible paths. The second term, called "coherent" intensity, is the interference term between wave propagation through different paths p and q. After an ensemble average on medium realizations, if scatterers are randomly placed and non-correlated, the interference term should vanish and only the incoherent term remains. When $R = S$ and at least two scatterers are involved, the coherent term can resist the ensemble average. Then, if multiple scattering occurs in the medium, the intensity on the source element is twice the baseline intensity recorded on a location different to the source. This intensity enhancement is often referred to as the coherent backscattering cone or coherent backscattered peak.

In this configuration, let us denote a first path $p1 = (S \longrightarrow S1 \longrightarrow S2 \longrightarrow S)$. Its reciprocal path is $p2 = (S \longrightarrow S2 \longrightarrow S1 \longrightarrow S)$. There are no phase difference between these two paths: the wave travel exactly the same distance, but in the inverse direction. Their intensity is the sum of their two individual intensities. This is the core of coherent backscattering: this intensity summation is only valid on the source element. Therefore, the average of the "coherent" term do not reduce to zero: the reciprocal paths remain and lead to a second term which has the same value than the incoherent intensity. The intensity on the source element is twice the "baseline" intensity recorded on a location different to the source. This intensity enhancement is often referred to as the coherent backscattering cone or coherent backscattered peak.

In this study, the coherent backscattering effect is used as a binary indicator: if observed at a certain time and frequency, multiple scattering occurs. On the contrary, the absence of coherent backscattering cone means that single scattering dominates.

Same data than the previous experiments were used. The average intensity was computed from the following configuration: the central element of the transducer fires a wave on the medium, and all transducer's elements record the backscattered wave. This process is iterated over several medium realizations, and for two probe angle: 0° and 90° as defined before.

The averaged intensity is computed on temporal windows

$$I_j^T = \sum_{medium\ realisation} |k_{N/2,j}^T(\omega)|^2, \quad (17)$$

where j is the receiving element.

An intensity enhancement is observed in TA6V in the perpendicular configuration Fig. 10 after 13 µs. This time is consistent with the single scattering proportion measurements and correspond to a time when multiple scattering already dominates. The

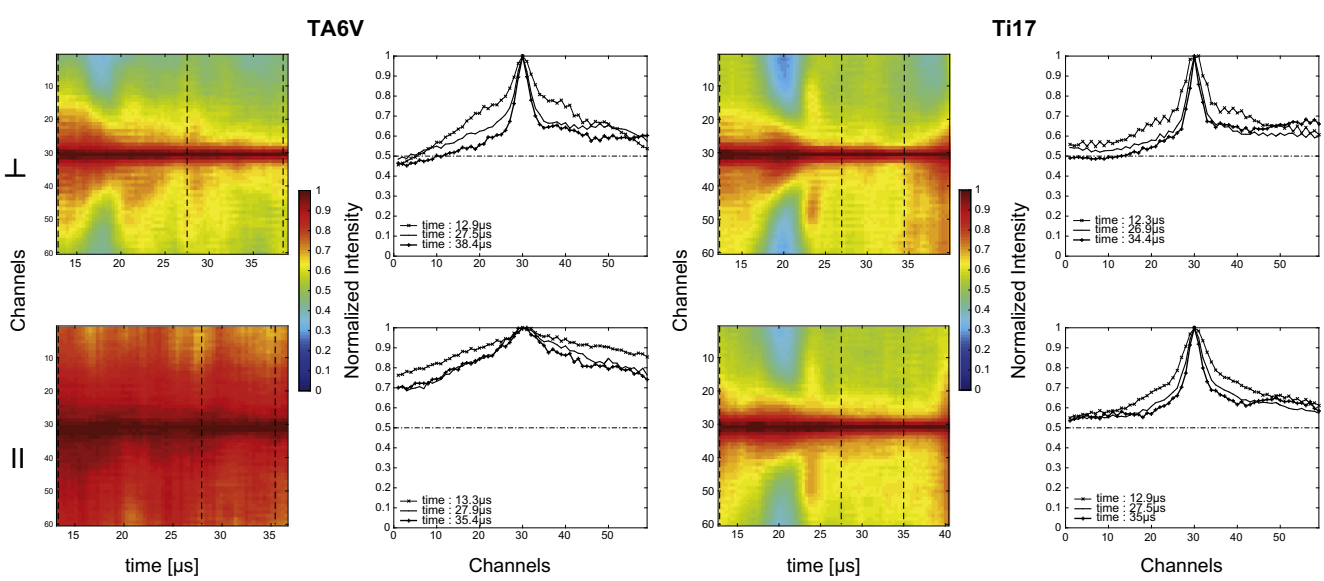

Fig. 10. Coherent backscattering cone measure on two samples with two probe configurations. (top left) TA6V in the perpendicular configuration, (bottom left) TA6V in the parallel configuration, (top right) Ti17 in the perpendicular configuration, (bottom right) Ti17 in the parallel configuration.

enhancement is weaker in the parallel configuration. The explanation is the same than in previous subsection: multiple scattering develops quicker in the transverse plane. Moreover, elements are aligned and thin in the transverse plane, leading to a good sampling of multiple scattering. This enhancement decreases in the parallel configuration: in the vertical plane, the field is coherent and elements integrate the multiple scattering on the transverse plane.

In the case of Ti17, an intensity enhancement is observed in both probe configurations after 13 μs. This is consistent with the multiple scattering estimator: strong multiple scattering is observed and is independent of probe angle.

6. Conclusion

Several indicators have been presented to determine the elongation direction of a complex media. These indicators result from different ways of post-processing the array response matrices for rotated linear transducer array. The first and simplest one, consists in averaging the backscattered intensity obtained on the diagonal of the array response matrix. By using the signal emitted and recorded by a single element of the array, this method could also be performed using a single transducer. The symmetry of the piezoelectric element is of importance: a circular element will lead to a constant backscattered intensity in function of the probe angle, a square element will lead to a 90° periodicity of the backscattered intensity curve, and a rectangular element will lead to a 180° periodicity. The elongation direction was identified as the probe angle corresponding to the minimum backscattered intensity. The second method uses the whole array response matrix, which samples the spatial coherence of the backscattered field to infer the single scattering proportion. In elongated medium, multiple scattering does not develop at the same speed in all directions. This effect, in conjunction with the element shape, appeared to be valuable for evaluating elongation direction in complex media. Moreover, this tool provides a straightforward method to quantify the multiple scattering and decide of the applicability of well-established models used for inspection design such as Thompson's ones [21,24]. Furthermore, results on multiple scattering were confirmed by the measure of the coherent backscattering cone. The measure of the phenomena also uses the array response matrix, through another post-processing. Because of its availability and its reasonable cost, we chose to use a linear transducer array. To go further, 2D matrix arrays could be used. They have already been used in medical imaging to perform ultrafast heart fiber orientation estimation [55]. Results of this article could be replicated without turning the linear phased array by using this type of matrix array.

Acknowledgement

The authors are grateful to A. Aubry for helpful discussions on multiple scattering and random matrices. The authors would like to thank the company SAFRAN and its corporate research center SAFRAN Tech for the funding of this research, and the company TIMET for providing the titanium samples.

References

[1] G.G. Lutjering, J. Williams, Titanium, second Ed., 2007. http://dx.doi.org/10.1007/978-3-540-73036-1.
[2] J.P. Bellot, D. Ablitzer, B. Foster, A. Mitchell, S. Hans, E. Hess, Dissolution of hard-alpha inclusions in liquid titanium alloys, Metall. Mater. Trans. B 28 (6) (1997) 1001–1010, https://doi.org/10.1007/s11663-997-0054-y.
[3] J.L. Henry, S.D. Hill, J.L. Schaller, T.T. Campbell, Nitride inclusions in titanium ingots: a study of possible sources in the production of magnesium-reduced sponge, Metall. Trans. 4 (8) (1973) 1859–1864, https://doi.org/10.1007/BF02665413.
[4] G. Ghazal, P. Chapelle, A. Jardy, J. Jourdan, Y. Millet, Dissolution of high density inclusions in titanium alloys, ISIJ Int. 52 (1) (2012) 1–9, https://doi.org/10.2355/isijinternational.52.1.
[5] W.P. Mason, H.J. Mcskimin, Attenuation and scattering of high frequency sound waves in metals et glasses, J. Acoust. Soc. Am. 19 (3) (1947) 464–473.
[6] I. Lifshits, G. Parkhomovski, On the theory of ultrasonic wave propagation in polycrystals, Zh. Eksp. Teor. Fiz 20 (1) (1950) 175–182.
[7] L. Merkulov, Investigation of ultrasonic scattering in metals, Sov. Phys.-Tech. Phys. 1 (1) (1956) 59–69.
[8] A. Bhatia, Scattering of high frequency sound waves in polycrystalline material, J. Acoust. Soc. Am. 464 (1947) (1959) 16–23.
[9] E.P. Papadakis, Grain-size distribution in metals and its influence on ultrasonic attenuation measurements, J. Acoust. Soc. Am. 33 (11) (1961) 1616, https://doi.org/10.1121/1.1908517.
[10] E.P. Papadakis, Rayleigh and stochastic scattering of ultrasonic waves in steel, J. Appl. Phys. 34 (2) (1963) 265–269, https://doi.org/10.1063/1.1702596.
[11] F.E. Stanke, G.S. Kino, A unified theory for elastic wave propagation in polycrystalline materials, J. Acoust. Soc. Am. 75 (3) (1984), https://doi.org/10.1121/1.390577.
[12] J.B. Keller, Stochastic equation and wave propagation in ranom media, Stoch. Process. Math. Phys. Eng. 16 (1980) 145.
[13] S. Hirsekorn, The scattering of ultrasonic waves by polycrystals, J. Acoust. Soc. Am. 72 (1982).
[14] S. Hirsekorn, The scattering of ultrasonic waves by multiphase polycristals, J. Acoust. Soc. Am. 83 (4) (1988) 1231–1242.
[15] J.A. Turner, R.L. Weaver, Radiative transfer and multiple scattering of diffuse ultrasound in polycristalline media, J. Acoust. Soc. Am. 96 (1994) 3675–3683.
[16] J.A. Turner, Elastic wave propagation and scattering in heteronegeous anisotropic media, Text. Polycrystal. Mater. 106 (2) (1999) 541–552.
[17] P. Panetta, F.J. Margetan, I. Yalda, R.B. Thompson, Ultrasonic attenuation measurements in jet-engine titanium alloys 15 (1996) 1525–1532.
[18] P.D. Panetta, R.B. Thompson, Ultrasonic attenuation in duplex titanium alloys, Rev. Progr. Quant. Nondestruct. Eval. 18 (1999) 1717–1724.
[19] S. Ahmed, R.B. Thompson, Influence of columnar microstructure on ultrasonic backscattering, Rev. Progr. Quant. Nondestruct. Eval. 14 (1995) 1617–1624.
[20] Y.K. Han, R.B. Thompson, Ultrasonic backscattering in duplex microstructures: theory and application to titanium alloys, Metall. Mater. Trans. A 28 (1) (1997) 91–104, https://doi.org/10.1007/s11661-997-0085-7.
[21] R.B. Thompson, F.J. Margetan, P. Haldipur, L. Yu, A. Li, P. Panetta, H. Wasan, Scattering of elastic waves in simple and complex polycrystals, Wave Motion 45 (5) (2008) 655–674, https://doi.org/10.1016/j.wavemoti.2007.09.008.
[22] F.J. Margetan, P. Panetta, R.B. Thompson, Ultrasonic signal attenuation in engine grade titanium alloy, Rev. Progr. Quant. Nondestruct. Eval. 17 (1998) 1469–1476.
[23] P.D. Panetta, R.B. Thompson, F.J. Margetan, Use of electron back scatter diffraction in understanding texture and the mechanism of back scattered noise generation in titanium alloys, Rev. Quant. Nondestr. Eval. 17 (1998) 89–96.
[24] F.J. Margetan, L. Yu, R.B. Thompson, Computation of grain-noise scattering coefficients for ultrasonic pitch/catch inspections of metals, AIP Conf. Proc. 760 (2005) (2005) 1300–1307, https://doi.org/10.1063/1.1916822.
[25] J.H. Rose, Theory of Ultrasonic backscatter from multiphase polycrystalline solids, Rev. Progr. Quant. Nondestruct. Eval. 32 (7) (1993), https://doi.org/10.1080/713821795, 747-747.
[26] J. Li, L. Yang, S.I. Rokhlin, Effect of texture and grain shape on ultrasonic backscattering in polycrystals, Ultrasonics 54 (7) (2014) 1789–1803, https://doi.org/10.1016/j.ultras.2014.02.020.
[27] O. Lobkis, L. Yang, J. Li, S. Rokhlin, Ultrasonic backscattering in polycrystals with elongated single phase and duplex microstructures, Ultrasonics 52 (6) (2011) 694–705, https://doi.org/10.1016/j.ultras.2011.12.002.
[28] L. Yang, O.I. Lobkis, S.I. Rokhlin, Shape effect of elongated grains on ultrasonic attenuation in polycrystalline materials, Ultrasonics 51 (6) (2011) 697–708, https://doi.org/10.1016/j.ultras.2011.02.002.
[29] L. Yang, J. Li, S. Rokhlin, Ultrasonic scattering in polycrystals with orientation clusters of orthorhombic crystallites, Wave Motion 50 (8) (2013) 1283–1302, https://doi.org/10.1016/j.wavemoti.2013.06.003.
[30] B. Lan, M. Lowe, F.P.E. Dunne, Experimental and computational studies of ultrasound wave propagation in hexagonal close-packed polycrystals for texture detection, Acta Mater. 63 (2014) 107–122, https://doi.org/10.1016/j.actamat.2013.10.012.
[31] A. Van Pamel, C.R. Brett, P. Huthwaite, M.J.S. Lowe, Finite element modelling of elastic wave scattering within a polycrystalline material in two and three dimensions, J. Acoust. Soc. Am. 138 (4) (2015) 2326–2336, https://doi.org/10.1121/1.4931445.
[32] A.V. Pamel, G. Sha, S.I. Rokhlin, M.J.S. Lowe, Finite-element modelling of elastic wave propagation and scattering within heterogeneous media, Proc. R. Soc. A 473(2197) 20160738 (The Royal Society). http://dx.doi.org/10.1098/rspa.2016.0738.
[33] A. Moreau, L. Toubal, P. Bocher, M. Humbert, E. Uta, N. Gey, Evaluation of macrozone dimensions by ultrasound and EBSD techniques, Mater. Charact. 75 (2013) 115–128, https://doi.org/10.1016/j.matchar.2012.09.011.
[34] L. Toubal, P. Bocher, A. Moreau, D. Lévesque, Macroregion size measurements in bimodal titanium forgings using two-dimensional autocorrelation method, Metall. Mater. Trans. A 41 (3) (2010) 744–750, https://doi.org/10.1007/s11661-009-0128-3.

[35] M.D. Russen, S.P. Neal, Experimental evidence of single and multiple scattering in polycrystalline materials, Rev. Progr. Quant. Nondestruct. Eval. 16 (1) (1997) 1521–1528, https://doi.org/10.1007/978-1-4615-5947-4_199.
[36] A. Derode, M. Fink, Partial coherence of transient ultrasonic fields in anisotropic random media: application to coherent echo detection, J. Acoust. Soc. Am. 101 (2) (1997) 690–704, https://doi.org/10.1121/1.417960. http://scitation.aip.org/content/asa/journal/jasa/101/2/10.1121/1.417960.
[37] C. Prada, S. Manneville, D. Spoliansky, M. Fink, Decomposition of the time reversal operator: detection and selective focusing on two scatterers, J. Acoust. Soc. Am. 99 (4) (1996) 2067, https://doi.org/10.1121/1.415393.
[38] C. Holmes, B.W. Drinkwater, P.D. Wilcox, Post-processing of the full matrix of ultrasonic transmit receive array data for non-destructive evaluation, NDT & E Int. 38 (2005) 701–711, https://doi.org/10.1016/j.ndteint.2005.04.002.
[39] A. Aubry, A. Derode, Random matrix theory applied to acoustic backscattering and imaging in complex media, Phys. Rev. Lett. 102 (2009) 1–4, https://doi.org/10.1103/PhysRevLett.102.084301.
[40] A. Derode, P. Roux, M. Fink, Robust acoustic time reversal with high-order multiple scattering, Phys. Rev. Lett. 75 (23) (1995) 4206–4209, https://doi.org/10.1103/PhysRevLett.75.4206.
[41] V. Mamou, Caractérisation ultrasonore d' échantillons hétérogènes multiplement diffuseurs, PhD thesis, Université Paris Diderot, 2005 (in French).
[42] A. Tourin, A. Derode, P. Roux, B. van Tiggelen, M. Fink, Time-dependent coherent backscattering of acoustic waves, Phys. Rev. Lett. 79 (2) (1997) 3637–3639, https://doi.org/10.1103/PhysRevLett.79.3637.
[43] A. Tourin, A. Derode, A. Peyre, M. Fink, Transport parameters for an ultrasonic pulsed wave propagationg in a multiple scattering medium, J. Acoust. Soc. Am. 108 (2) (2000) 503–512.
[44] F. Margetan, M. Gigliotti, L. Brashe, W. Leach, Fundamental studies: Inspection Properties for Engine Titanium Alloys, FAA Report (December). doi: <http://oai.dtic.mil/oai/oai?verb=getRecord&metadataPrefix=html&identifier=ADA411492>.
[45] A. Schwartz, M. Kumar, B. Adams, D. Field, Electron Backscatter Diffraction in Materials Science, Springer, New York, 2009. http://www.springer.com/in/book/9780387881355.
[46] F.J. Margetan, R.B. Thompson, I. Yalda-Mooshabad, Backscattered microstructural noise in ultrasonic toneburst inspections, J. Nondestr. Eval. 13 (3) (1994) 111–136, https://doi.org/10.1007/BF00728250.
[47] F.J. Margetan, R.B. Thompson, I. Yalda-Mooshabad, Ultrasonic propagation and scattering in duplex microstructures with application to titanium alloys, Rev. Progr. Quant. Nondestruct. Eval. 12 (1993) 1735–1742.
[48] F.J. Margetan, K.Y. Han, I. Yalda-mooshabad, S. Goettsch, R.B. Thompson, The practical application of grain noise model in titanium billets and forging, Rev. Progr. Quant. Nondestruct. Eval. 14 (1995) 2129–2136.
[49] S. Ahmed, M.T. Anderson, Task 1 Final Report: Theoretical Mathematical Modeling of Ultrasonic Wave Propagation in Anisotropic Polycrystalline Stainless Steels, US Department of Energy (PNNL-18363), 2009.
[50] L. Yang, J. Li, O.I. Lobkis, S.I. Rokhlin, Ultrasonic propagation and scattering in duplex microstructures with application to titanium alloys, J. Nondestr. Eval. 31 (3) (2012) 270–283, https://doi.org/10.1007/s10921-012-0141-0.
[51] K. Sakai, K. Yamamoto, K. Takagi, Observation of acoustic coherent backscattering, Phys. Rev. B 56 (17) (1997) 930–933.
[52] M. Vithana, L. Asfaw, D. Johnson, Coherent backscattering of light in a nematic liquid crystal, Phys. Rev. Lett. 64 (23) (1990) 2304–2308.
[53] L. Margerin, M. Campillo, B.a. Van Tiggelen, Coherent backscattering of acoustic waves in the near field, Geophys. J. Int. 145 (2001) 593–603, https://doi.org/10.1046/j.1365-246X.2001.01400.x.
[54] G. Bayer, T. Niederdränk, Weak localization of acoustic waves in strongly scattering media, Phys. Rev. Lett. 70 (25) (1993) 3884–3887, https://doi.org/10.1103/PhysRevLett.70.3884.
[55] C. Papadacci, V. Finel, J. Provost, O. Villemain, P. Bruneval, J.L. Gennisson, M. Tanter, M. Fink, M. Pernot, Imaging the dynamics of cardiac fiber orientation in vivo using 3D Ultrasound Backscatter Tensor Imaging, Sci. Rep. 7 (1) (2017) 830.